Journal of Magnetism and Magnetic Materials 538 (2021) 168307

Contents lists available at ScienceDirect

Journal of Magnetism and Magnetic Materials

journal homepage: www.elsevier.com/locate/jmmm

Synthesis, structural, and magnetic properties of Heusler-type $Mn_{2-x}Fe_{1+x}Ge$ ($0.0 \leq x \leq 1.0$) alloys

Anil Aryal [a,*], Igor Dubenko [a], J. Zamora [b], J.L. Sánchez Llamazares [b,*], C.F. Sánchez-Valdés [c], Dipanjan Mazumdar [a], Saikat Talapatra [a], Shane Stadler [d], Naushad Ali [a]

[a] Department of Physics, Southern Illinois University, Carbondale, IL 62901, USA
[b] Instituto Potosino de Investigación Científica y Tecnológica A.C, Camino a la Presa San José 2055 Col. Lomas 4ª, San Luis Potosí, S.L.P. 78216, Mexico
[c] Departamento de Física y Matemáticas, División Multidisciplinaria en Ciudad Universitaria, Instituto de Ingeniería y Tecnología, Universidad Autónoma de Ciudad Juárez (UACJ), Ciudad Juárez, Chihuahua 32310, Mexico
[d] Department of Physics & Astronomy, Louisiana State University, Baton Rouge, LA 70803, USA

ARTICLE INFO

Keywords:
Heusler-type $Mn_{2-x}Fe_{1+x}Ge$ alloys
Crystal structure
Magnetization
Curie temperature

ABSTRACT

Bulk $Mn_{2-x}Fe_{1+x}Ge$ ($0.0 \leq x \leq 1.0$) alloys have been synthesized by arc-melting followed by a low temperature homogenization thermal annealing, whereas for comparison purposes the Mn_2FeGe alloy was also produced in ribbon form by rapid solidification. A study of the structural and magnetic properties is presented. Contrary to theoretical predictions, Mn_2FeGe crystallizes in a hexagonal DO_{19} crystal structure (space group *P63/mmc*) and orders ferromagnetically with a saturation magnetization (M_S) value of ~1.7 μ_B/f.u. in the ground state. With the substitution of Fe for Mn in bulk $Mn_{2-x}Fe_{1+x}Ge$, we observed an increase in the FM interactions with a maximum M_S value of 5.1 μ_B/f.u. for $x = 1.0$, and a significant progressive increase in the Curie temperature (T_C) in a wide range spanning ~200 K to over 400 K.

1. Introduction

Heusler alloys have the general composition X_2YZ (i.e., 2:1:1), where X and Y are 3d transition elements, and Z is a main group element. Stoichiometric Heusler alloys with composition 2:1:1 commonly crystallize in a highly-ordered cubic $L2_1$-type (Cu_2MnAl prototype) crystal structure with the $Fm\bar{3}m$ (225) space group. In this case, X, Y, and Z atoms occupy the following Wyckoff positions: X at the 8c site $\left(\frac{1}{4},\frac{1}{4},\frac{1}{4}\right)$, Y at the 4b site $\left(\frac{1}{2},\frac{1}{2},\frac{1}{2}\right)$, and Z at the 4a site (0,0,0) [1]. However, if the valence of the Y element is higher than that of the element in the X sites, the alloy crystallizes in an inverse Heusler Hg_2CuTi-type crystal structure with the space group Fm-3 m No. (216) [2,3]. The inverse-Heusler structure can be derived from the normal one by interchanging one of the X atoms with a Y atom. In that case, the Z and Y elements occupy the (0, 0, 0) and $\left(\frac{1}{4},\frac{1}{4},\frac{1}{4}\right)$ Wyckoff positions, respectively, while the X elements occupy the $\left(\frac{3}{4},\frac{3}{4},\frac{3}{4}\right)$ and $\left(\frac{1}{2},\frac{1}{2},\frac{1}{2}\right)$ positions. Additionally, non-cubic Heusler alloys, with hexagonal or tetragonal crystal structures and high spin-polarizations, have also been recently reported [4–7].

Among all families of Heusler-type magnetic alloys, those based on Mn have attracted special attention in the last 20 years due to the large variety of physical phenomena and effects found in different alloy systems such as magnetic shape memory, magnetic superelasticity, magnetoresistance, half-metallicity, metamagnetism, and magnetocaloric, anomalous Hall, and exchange bias effects [8]. As the exact physical mechanisms responsible for all the aforementioned physical phenomena are not yet fully understood, experimental studies on known and newly synthesized compounds are an essential source of information.

Recent first-principles theoretical calculations carried out by *Ma et al.* identified inverse Heusler Mn_2FeZ-type phases with Z = Al, Si, Ge, Ga, In, Sn, and Sb [3]. Even though theoretical studies predict their expected basic structural and magnetic properties, they must be experimentally confirmed or refuted since discrepancies may often appear. A recent example is that of the Mn_2FeAl compound; whereas theoretical findings suggested an inverse $L2_1$-type cubic structure, it adopts a geometrically frustrated cubic β-Mn structure (space group $P4_132$) [9].

* Corresponding authors.
E-mail addresses: aryalanil@siu.edu (A. Aryal), jose.sanchez@ipicyt.edu.mx (J.L. Sánchez Llamazares).

https://doi.org/10.1016/j.jmmm.2021.168307
Received 29 August 2020; Received in revised form 13 July 2021; Accepted 14 July 2021
Available online 21 July 2021

In the case of Mn_2FeGe, which is the main focus of the present work, theoretical calculations predict that it is a half-metallic ferrimagnetic compound with the inverse Heusler-type cubic crystal structure [3,10]. Instead, it will be shown here that it crystallizes in the same hexagonal DO_{19} crystal structure as does Fe_2MnGe [6,11]. Even though the understanding of spin-polarization and related properties, such as half-metallicity, require a detailed investigation of the band structure, there are other important characteristics that make hexagonal Heusler-type alloys exciting for spintronics applications as they inherently show volume perpendicular magnetic anisotropy (PMA) which is suitable for spin-transfer torque magnetic random-access memory (STT-MRAM) devices [4–7,10,12,13]. This contrasts with cubic Heusler alloys that, by definition, do not exhibit volume PMA. We additionally prepared the series $Mn_{2-x}Fe_{1+x}Ge$ with $0.2 \leq x \leq 1.0$ with the aim to study the trend of saturation magnetization M_S and Curie temperature T_C with the progressive replacement of Mn by Fe (i.e., going from the Mn_2FeGe to Fe_2MnGe).

2. Experimental details

Bulk alloys with nominal composition $Mn_{2-x}Fe_{1+x}Ge$ with $x = 0.0$, 0.2, 0.4, 0.6, 0.7, 0.8, and 1.0, were produced by arc-melting from high-purity elements (≥99.99 %) in an ultra-high purity (UHP) argon atmosphere. To ensure good homogeneity, the samples were flipped and re-melted four times and then thermally annealed under high vacuum (~10^{-6} Torr) at 923 K (650 °C) for 48 h. The annealed bulk Mn_2FeGe ingot was cut into two halves using a low-speed diamond-wheel saw. One piece was studied in bulk form, whereas the other was used to fabricate melt-spun ribbons. The rapid solidification process was carried out in an Edmund Bühler model SC melt spinner system under a UHP He atmosphere at a linear speed of the rotating copper wheel of 10 ms^{-1}. The obtained melt-spun ribbon flakes were studied both in the as-solidified (AS) state and after a thermal annealing (ANN) under the same conditions as those of the bulk.

The phase constitutions and crystal structures at room temperature were studied by powder X-ray diffraction (XRD) using a high-resolution Rigaku Smartlab diffractometer (Cu-$K_{\alpha 1}$ radiation). Rietveld refinement of the XRD patterns for the AS and ANN Mn_2FeGe ribbon samples were carried out using MATCH software which is based on FULLPROF software [14]. The microstructures and the elemental composition of the melt-spun ribbons were studied in an FEI Helios NanoLab 600 system; the system is equipped with an energy dispersive spectroscopy (EDS) system from EDAX.

Magnetization measurements on bulk samples were performed using a SQUID magnetometer in the temperature range from 5 to 380 K applying a maximum magnetic field $\mu_o H = 5$ T. The magnetic properties of the ribbons were also studied in a 9 T Quantum Design PPMS® Dynacool® system using the vibrating sample magnetometry (VSM) option from 10 to 400 K in fields up to $\mu_o H = 5$ T. The magnetization as a function of temperature was measured following zero-field-cooled (ZFC) and field-cooled (FC) protocols with a temperature sweep rate of 1.0 K/min. The temperature of the magnetic phase transition (T_C) was determined from the minimum of the dM/dT vs. T curves. The electrical resistivity ρ for the bulk Mn_2FeGe alloy was measured using the four-probe method in a SQUID magnetometer from 10 to 380 K at a temperature sweep rate of 3.0 $Kmin^{-1}$ with and without the application of a static magnetic field of 5 T. Measurements were done on a parallelepiped-shaped specimen cut from the bulk sample.

3. Results and discussions

3.1. Bulk and melt-spun ribbon samples of stoichiometric Mn_2FeGe: structural and magnetic characterization.

Fig. 1(a) through (e) show the SEM micrographs of the typical microstructures of polycrystalline as-solidified (AS) and annealed (ANN) ribbons. Both samples showed a similar topography at the surfaces that make contact (CS) and non-contact (NCS) with the wheel surface. Samples are mainly composed of elongated crystals with hexagonal cross-sections whose major lengths seems to be randomly oriented with respect to both ribbon surfaces (reflecting a higher grain growth rate along the hexagonal c axis in comparison to the basal plane), plus small white precipitated particles as a minor phase. The characteristic EDS microanalysis spectra for the two common and distinct zones observed in both samples are shown in Fig. 1(f) and (g). The presence of carbon in the spectra comes from the conductive carbon tape used to attach the samples to the aluminum sample holder. After a large number of EDS analyses were carried out on both ribbon surfaces, it was found that the matrix shows an elemental chemical composition (Mn: Fe: Ge) close to 2:1:1 with 53:26:21 at. % and 52:25:23 at. % for AS and ANN samples, respectively. In contrast, the EDS spectra of the observed white particles reveal that they are oxygen-rich. Their average elemental compositions (O:Mn:Fe:Ge) were found to be 42:56:1:1 at. % and 59:36:3:2 at. % for in the AS and ANN ribbons samples, respectively.

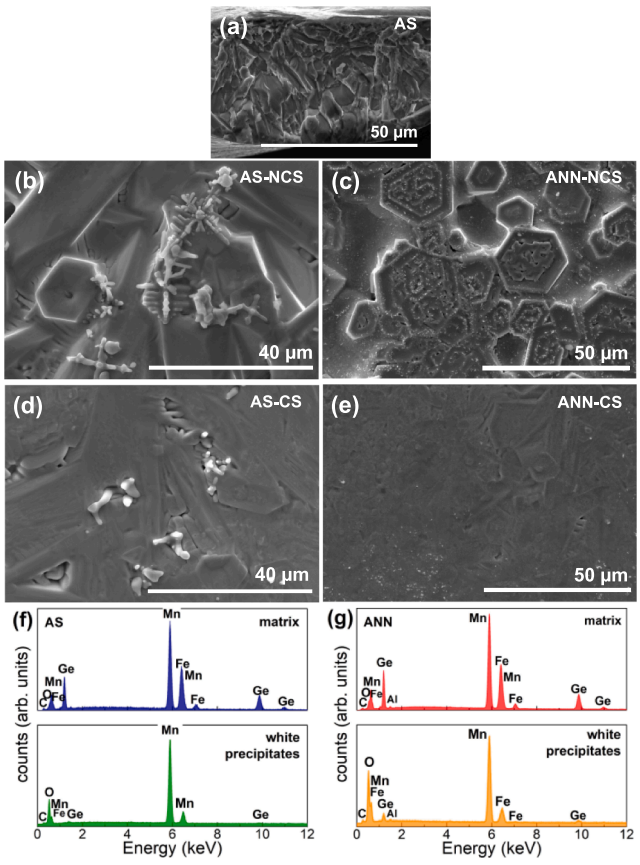

Fig. 1. (a), (b), and (d) SEM micrographs show the characteristic microstructure of as-solidified (AS) ribbons at the cross-section, and the surfaces that do not make contact (NCS) and make contact (CS) with the copper wheel during solidification, respectively. The respective images for the annealed ribbons are shown in (c) and (e). EDS spectra for the two distinct phases observed in AS and ANN ribbons: as-quenched (f) and annealed (g) ribbons.

Dot EDS maps, presented in Fig. 2, provide further information about element distribution. The pictures shown from Fig. 2(b) to (e) prove that the white precipitates are composed of Mn and O, whereas the matrix is comprised of Mn, Fe, and Ge. Considering that the ribbons were obtained from a piece cut from the original bulk arc-melted ingot, the determination of the elemental chemical composition by EDS led us to conclude that the formation of oxide comes from the sample during the casting process due to the high susceptibility of the manganese to oxidize.

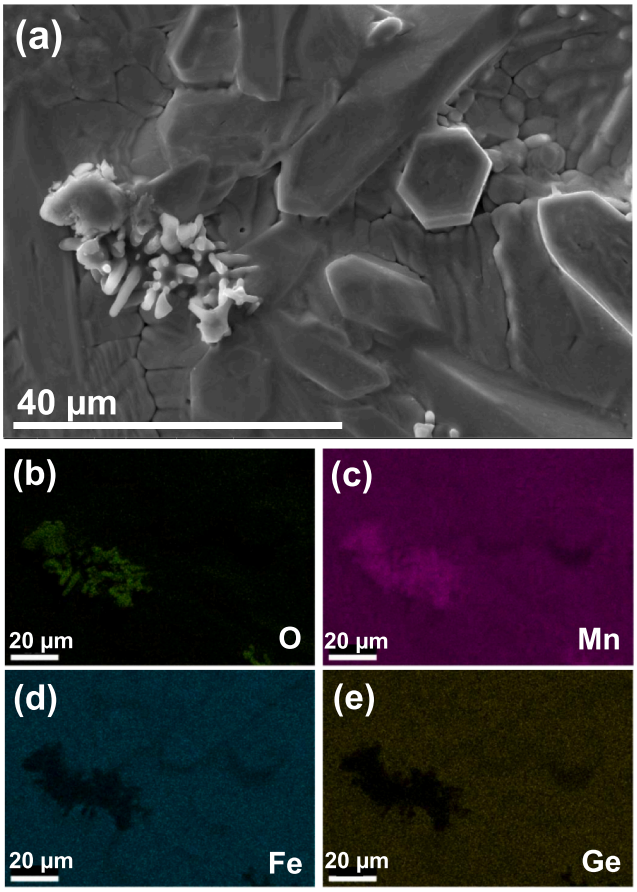

Fig. 2. SEM micrograph (a), and dot EDS element mapping images of O (b), Mn (c), Fe (d), and Ge (e) for as-solidified (AS) ribbon samples.

Fig. 3 compares the powder XRD patterns of the bulk and melt-spun Mn_2FeGe samples. The major phase in the three patterns was successfully indexed based on a hexagonal DO_{19} crystal structure with the *P63/mmc* space group. However, the appearance of additional Bragg peaks in the pattern for the bulk alloy reveals the presence of a secondary phase

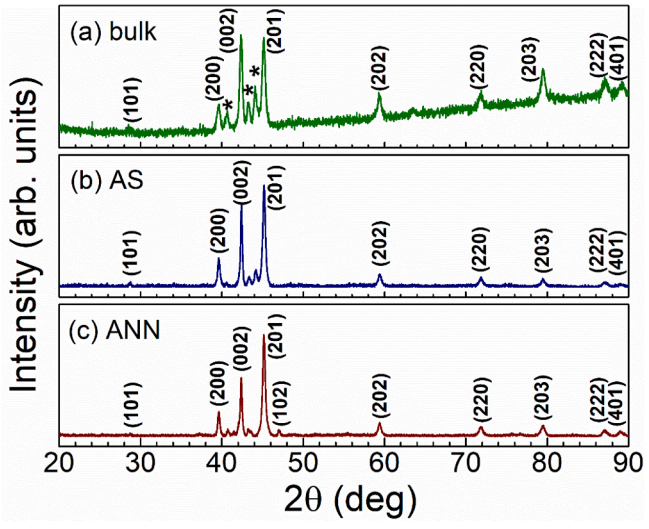

Fig. 3. X-ray powder diffraction patterns for (a) bulk, (b) as-solidified, and (c) thermally annealed melt-spun Mn_2FeGe ribbons. The peaks indicated by asterisks reveal the formation of oxides as a secondary phase. The XRD peak indexing was based on the hexagonal DO_{19} crystal structure.

with a total fraction of about 20 % (roughly estimated from the XRD peak intensities), which correspond to those of Mn-oxides, which is consistent with the dot EDS maps analysis. It should be noted that the intensities of the diffraction peaks coming from the second phase are reduced significantly in both AS and ANN samples, suggesting that a proper choice of processing parameters using this technique may lead to the production of a single-phase DO_{19} crystal structure.

The Rietveld refinement of the XRD patterns for AS and thermally annealed ribbons are shown in Fig. S1. Notice that the intensity of one of the XRD peaks does not match with the corresponding simulated peak for both samples, a fact that is attributed to the partial crystallographic texture of the samples. The XRD fitting, performed on the basis of the hexagonal DO_{19} crystal structure with space group *P63/mmc*, provided the lattice parameters $a = 5.2533 \pm 0.0002$ Å, $c = 4.2645 \pm 0.0003$ Å for as-solidified ribbons, and $a = 5.2536 \pm 0.0002$ Å, $c = 4.2670 \pm 0.0003$ Å for thermally annealed ribbons. These values are consistent with those determined for the bulk sample: $a = 5.2528 \pm 0.0002$ Å, $c = 4.2626 \pm 0.0003$ Å. It must be highlighted that, contrary to the theoretical prediction of a highly symmetric cubic structure [3,10], the XRD patterns show that Mn_2FeGe adopts a low-symmetry hexagonal structure. Notice that this is consistent with both the hexagonal cross-sections observed in the grains (see Fig. 1) and the crystal symmetry reported for Mn_3Ge which can be considered as the parent compound [15]. Thus, further theoretical investigations are needed in order to understand the origin of the hexagonal phase stability experimentally found for the Mn_2FeGe alloy.

The isothermal magnetization $M(\mu_o H)$ curves at 10 K up to $\mu_o H = 5$ T for Mn_2FeGe bulk and AS ribbon samples are shown in Fig. 4(a). $M(\mu_o H)$ curves show that polycrystalline Mn_2FeGe exhibits maximum magnetization values of about 37 Am^2kg^{-1} (~1.6 μ_B/f.u.) for bulk and 39 Am^2kg^{-1} (~1.7 μ_B/f.u.) for ribbons (i.e., almost equal values) at $\mu_o H = 5$ T. In Ref. [6], a larger magnetization value of Fe_2MnGe Heusler alloys (with the same hexagonal DO_{19} structure) at $T = 5$ K have been reported to be about 117 Am^2kg^{-1} (~5 μ_B/f.u.) at 5 T. Considering that the maximum Mn-magnetic moment is 5 μ_B, the magnetization of the Mn_2FeGe compound should be larger than that of Fe_2MnGe assuming a collinear ferromagnetic state. However, the observed $M_0 \sim 33$ Am^2kg^{-1} (~1.4 μ_B/f.u.) is much smaller for Mn_2FeGe compound. Thus, considering the significant susceptibility in high magnetic field ($\chi_H = (M(\mu_o H) - M_0)/(\mu_o H)$) exhibited by Mn_2FeGe (see in Fig. 4(a)) and the small magnetic moment of Mn (of about 1μ_B/f.u.), one can conclude that this compound is in a non-collinear ferromagnetic state.

In order to further confirm the magnetic structure in the ground state, the effective magnetic moment (μ_{eff}) in the paramagnetic (PM) region was calculated from inverse susceptibility $\chi^{-1}(T)$ data using the relation $(\mu_{eff}/\mu_B)^2 = (3\ k_B / N)\ C_m \approx 8\ C_m$, where C_m is the molar Curie constant [16]. A μ_{eff} value of 5.16 μ_B/f.u. was found using this calculation. Using $\mu_{eff} = g\ [J(J+1)]^{1/2}\mu_B$, the saturation magnetization value was calculated using $M_0 = gJ\ \mu_B$ [16], and $g = 2$. The calculated value of M_0 was found to be 4.3 μ_B/f.u. for the Mn_2FeGe compounds. Thus, magnetic moment of this compound should be 4.3 μ_B/f.u. at zero magnetic field and temperature. Comparing the two values of the magnetic and effective moments obtained from $M(\mu_o H)$ and $M(T)$ curves, 1.4 μ_B/f.u. and 4.3 μ_B/f.u., respectively, one can conclude that Mn_2FeGe is in a non-collinear ferromagnetic phase in the ground state.

Fig. 4(b) shows ZFC and FC $M(T)$ curves measured under static magnetic fields of 0.1 and 5 T for both bulk and AS and ANN melt-spun ribbons. For the latter, the $M(T)$ curves measured under a high magnetic field of 5 T are also included to show that the saturation magnetization and Curie temperature T_C do not change appreciably with the thermal treatment. The $dM(T)/dT$ versus T curves at 0.1 T are shown in the inset.

A magnetic transition to a PM state was observed in both the bulk system and the ribbons with Curie temperatures (T_C) of about 202 K and 190 K (ANN) −193 K (AS), respectively (estimated from the peak of the respective dM/dT vs T curves). Notice that, in the temperature interval of the magnetic transition, the low-field ZFC and FC $M(T)$ curves

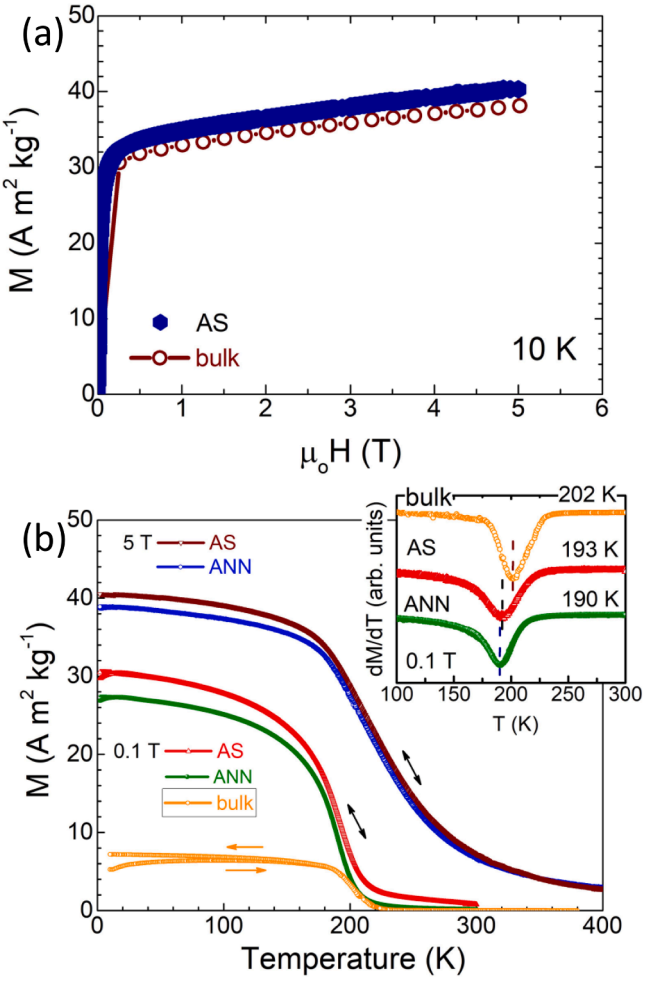

Fig. 4. (a) Isothermal magnetization $M(\mu_oH)$ curves at 10 K up to 5 T for bulk and AS Mn_2FeGe ribbon samples. (b) ZFC and FC temperature dependence of the magnetization $M(T)$ for bulk and melt-spun ribbon samples. Arrows in the graphs indicate whether the curve corresponds to a heating or cooling cycle. Inset: dM/dT as a function of T curves.

overlap, indicating full reversibility. Its second-order nature was confirmed by calculating the Arrott plots (i.e., M^2 as a function of μ_oH/M) [17]. Fig. S2(a) and (b) show the magnetization isotherms measured for bulk and ANN ribbon samples in the phase transition region. Taking as a reference the thermally annealed ribbons, Fig. S2(c) shows the computed Arrott plots. For a first-order transition, they should show an S shape, whereas for second-order their slopes are always positive with a concavity that changes from negative to positive when the magnetic state changes from the FM to paramagnetic state [17]. Hence, Fig. S2(b) confirms the second-order nature of the magnetic transition for the Mn_2FeGe alloy.

From the magnetization isotherms shown in Fig. S2 we also obtained, by the numerical integration of the Maxwell relation, the temperature dependence of the magnetic entropy change $\Delta S_M(T)$, across the ferromagnetic transition of this new Heusler system. The $\Delta S_M(T)$ curves for magnetic field change values $\mu_o\Delta H$ of 1 and 2 T for the bulk and ANN samples are shown in Fig. S3. $|\Delta S_M|^{max}$ reaches moderate to low values around T_C of 0.8 Jkg^{-1}K^{-1} and 0.9 Jkg^{-1}K^{-1} with $\mu_o\Delta H = 2$ T for bulk and thermally annealed ribbons, respectively. The low $|\Delta S_M|^{max}$ values are consistent with the broad magnetization decay and small magnetization change in the phase transition region. The most significant parameters that can be assessed from the $\Delta S_M(T)$ curves are listed in Table S1.

The temperature dependencies of the electrical resistivity $\rho(T)$ measured for the bulk Mn_2FeGe alloy at zero magnetic field (on heating and cooling) and at 5 T (on heating) are shown in Fig. 5. A typical metallic behavior (electron–electron scattering) was found at low temperature up to 50 K [see the $\rho(T) \sim T^2$ fitting at the inset of the Fig. 5]. An unusually large residual resistivity of $\rho_o = 559$ μΩ cm at $T = 10$ K and $\mu_oH = 0$ T was observed. The residual resistivity ratio (ρ300k-ρ10k) calculated from the zero-field $\rho(T)$ curve during heating, was found to be about 1.3. At higher temperatures, $\rho(T)$ was found to be linear with T. A change in the slope of the $\rho(T)$ curve was observed around 200 K which matches well with the measured T_C value (i.e., 202 K) obtained from the $M(T)$ measurements (see Fig. 4(b)). At temperatures $T < T_C$, the resistivity decreased rapidly due to magnetic ordering. According to Matthiessen's rule, the total resistivity in magnetic materials is given by $\rho(T) = \rho_o + \rho_{e-ph}(T) + \rho_{e-mag}(T) = \rho_o + AT + BT^2$, where ρ_o is the residual resistivity, $\rho_{e-ph}(T)$ is the resistivity due to electron–phonon scattering (with a linear T dependence), $\rho_{e-mag}(T)$ is the resistivity due to electron-magnon scattering (with a T^2 dependence), and A and B are constants. As the inset of Fig. 5 shows, at low temperatures the resistivity follows a T^2 law, indicating the dominance of magnetic scattering. On the other hand, the linear dependence of resistivity at high temperatures (i.e., $T > T_C$) indicates the dominance of electron–phonon scattering.

3.2. *Trend of saturation magnetizations and magnetic transitions for bulk $Mn_{2-x}Fe_{1+x}Ge$ alloys ($0.0 \le x \le 1.0$)*

Fig. 6 shows the X-ray powder diffraction patterns recorded for the bulk $Mn_{2-x}Fe_{1+x}Ge$ alloys with $x = 0.2$, 0.4, 0.6, and 1.0. The peak positions for all samples are consistent with the hexagonal DO_{19} crystal structure. However, refinement analysis could not be performed due to the dominant (002) texture observed in all the samples. According to our simulations, the (201) peak should be roughly four times as strong as the (002) and (200) peak, which is not the case in any sample. Such observations are similar to recent literature reports [6] and could be the result of the growth and annealing conditions. Analyzing the (200) and (002) peak positions of the $x = 1.0$ sample (Fe_2MnGe) provided $a = 5.21$ Å and $c = 4.24$ Å using the formula $\frac{1}{d^2} = \frac{4}{3a^2}\left(h^2 + k^2 + hk\right) + \frac{l^2}{c^2}$. These values are very close to the results reported in Keshavarz *et al.* [6].

A recent theoretical study by *Meng et al.* on the magnetic properties of hexagonal DO_{19} Fe_2MnGe (which is the endmember ($x = 1.0$) of the $Mn_{2-x}Fe_{1+x}Ge$ series) showed that the compound is ferromagnetic with a large *Ms* due to the large and parallel-coupled magnetic moments of Fe and Mn [11]. Isothermal magnetization $M(\mu_oH)$ curves measured at $T = 10$ K up to a magnetic field of 5 T for samples with $0.0 \le x \le 1.0$ are

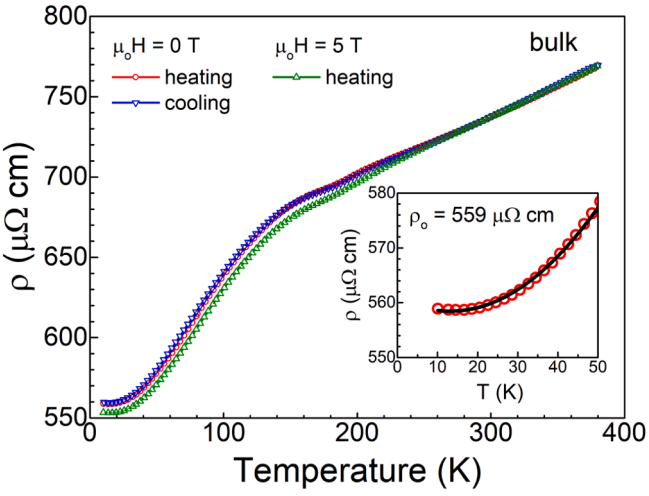

Fig. 5. Temperature dependence of the electrical resistivity for bulk Mn_2FeGe at $\mu_oH = 0$ T (on heating and cooling) and at 5 T (on heating). The inset shows that the resistivity follows a T^2 law at low temperature. The solid line in the inset is a guide for the eyes.

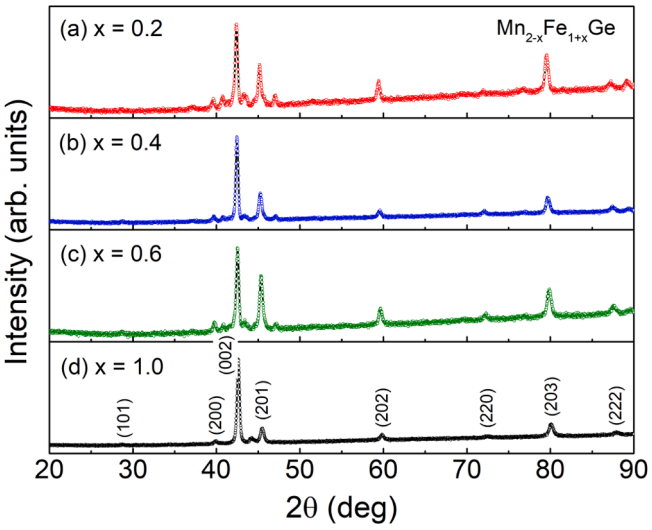

Fig. 6. X-ray powder diffraction patterns for bulk $Mn_{2-x}Fe_{1+x}Ge$ alloys with $0.2 \leq x \leq 1.0$. The peak indexing was based on the hexagonal DO_{19} crystal structure.

shown in Fig. 7(a). All compounds were found to exhibit ferromagnetic type of M(H) curves. As shown in the inset of Fig. 7(b), the saturation magnetization progressively increased from a small Fe concentration (x = 0.2), whereas for higher Fe concentrations (i.e., around x = 0.6 and over) a saturation trend in M_S was observed. Large M_S values were obtained in the $Mn_{2-x}Fe_{1+x}Ge$ alloys with a maximum of 5.1 μ_B/f.u. for $x = 1.0$, which is in good agreement with values reported in Refs. [6,11]. The results demonstrate the enhancement of ferromagnetism in the $Mn_{2-x}Fe_{1+x}Ge$ series when Fe gradually replaces Mn.

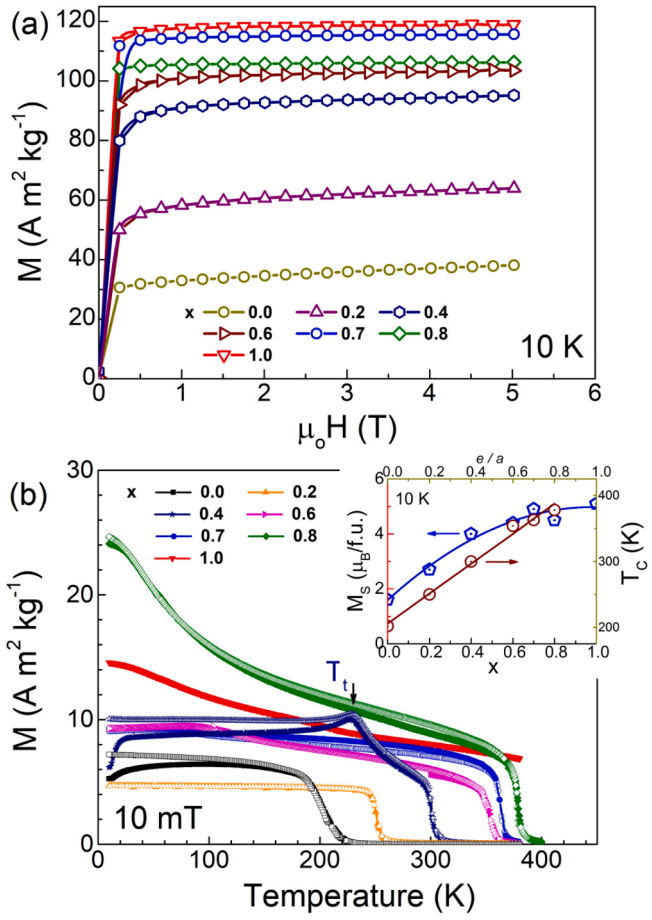

Fig. 7. Bulk $Mn_{2-x}Fe_{1+x}Ge$ alloys with $0.0 \leq x \leq 1.0$: (a) $M(\mu_oH)$ curves measured at $T = 10$ K up to 5 T. (b) $M(T)$ curves measured under a field of 10 mT following ZFC and FC cycles (denoted by solid and open symbols, respectively). Inset in (b): M_S and T_C with as a function of the Fe content (x) and the valence electron concentration (e/a). The lines are guides for the eyes.

It should be noted here that the maximum magnetic moment of the Mn- subsystem of about 5 μ_B/Mn (or 10 μ_B/f.u.) is much larger than that obtained from magnetization curves at 10 K. That the 3d magnetic subsystem of stoichiometric Mn_2FeGe demonstrates such a small value indicates that it is likely in a weak magnetic state. Therefore, neutron diffraction measurements should be done to determine the specific magnetic structure of the compounds.

The temperature dependence of the magnetization $M(T)$ for bulk $Mn_{2-x}Fe_{1+x}Ge$ ($0.0 \leq x \leq 1.0$) alloys measured under a magnetic field of 10 mT is shown in Fig. 7(b). A second-order magnetic transition (SOT) from a FM to PM state with a sharp drop in magnetization was observed at T_C for the series. An additional transition at $T_t = 238$ K was observed for the alloy with $x = 0.4$, probably indicating the occurrence of a spin reorientation transition. A shift in T_C to higher temperatures (from 200 K to above 400 K) was observed, suggesting an increase in FM interactions with Fe substitution. The variation of T_C with the Fe content and valence electron concentration (e/a) is shown in the inset of Fig. 7(b). Notice that T_C increased linearly with the increase of both Fe concentration and e/a ratio.

The temperature dependences of $\triangle S_M$ for $Mn_{2-x}Fe_{1+x}Ge$ alloys with $x = 0.2$ and 0.4, and for values of $\mu_o\Delta H$ of 1 and 2 T, are given in Fig. S4. They were also determined from sets of $M(\mu_oH)$ curves measured in the magnetic transition region of both alloys (not shown). $|\triangle S_M|^{max}$ reaches values of 1.2 $Jkg^{-1}K^{-1}$ and 1.5 $Jkg^{-1}K^{-1}$ at $\mu_o\Delta H = 2$ T for $x = 0.2$ and $x = 0.4$, respectively. A significant increase in the $|\triangle S_M|^{max}$ values at $\mu_o\Delta H = 2$ T from 0.8 $Jkg^{-1}K^{-1}$ (for the parent Mn_2FeGe) to 1.5 $Jkg^{-1}K^{-1}$ was observed in the Fe doped alloys.

4. Conclusion

In summary, the structural and magnetic properties of bulk and melt-spun ribbons of the stoichiometric Mn_2FeGe Heusler alloy were studied; in addition, the trend of the magnetic phase transitions and saturation magnetizations of bulk $Mn_{2-x}Fe_{1+x}Ge$ ($0.0 \leq x \leq 1.0$) alloys was investigated. Experimental results show that: (i) all samples crystallized in a hexagonal DO_{19} crystal structure with the space group *P63/mmc;* (ii) the magnetic behavior of the Mn-rich compounds may be described by a non-collinear ferromagnetic structure or/and a weak ferromagnetic state of the 3d-subsystem, resulting in a saturation magnetization of ~1.4 μ_B/f.u. in the ground state; and (iii) that the dominant mechanisms of the resistivity are electron–phonon and magnetic scattering below and above $T_C = 50$ K, respectively.

CRediT authorship contribution statement

Anil Aryal: Conceptualization, Data curation, Formal analysis, Investigation, Writing - original draft, Validation, Visualization. **Igor Dubenko:** Supervision, Methodology. **J. Zamora:** Investigation, Data curation, Validation. **J.L. Sánchez Llamazares:** Funding acquisition, Supervision. **C.F. Sánchez-Valdés:** Data curation, Supervison. **Dipanjan Mazumdar:** Software, Supervison, Funding acquisition. **Saikat Talapatra:** Funding acquisition, Supervision. **Shane Stadler:** Funding acquisition, Supervision. **Naushad Ali:** Funding acquisition, Supervision.

Declaration of Competing Interest

The authors declare that they have no known competing financial interests or personal relationships that could have appeared to influence the work reported in this paper.

Acknowledgments

This work was supported by the U.S. Department of Energy (DOE), Office of Science, Basic Energy Sciences (BES) under Awards No. DE-FG02-06ER46291 (SIUC) and DE-FG02-13ER46946 (LSU) and by SEP-CONACYT, Mexico, under project A1-S-37066. AA and DM would like to acknowledge an NSF CAREER grant (ECCS, Award # 1846829) for support of this work. The authors also acknowledge financial support received from Laboratorio Nacional de Investigaciones en Nanociencias y Nanotecnología (LINAN, IPICyT) and the technical support of M.Sc. B. A. Rivera Escoto and M.Sc. A.I. Peña Maldonado. J. Zamora is grateful to CONACyT-Mexico for supporting his postdoctoral position at IPICyT. C. F. Sánchez-Valdés is grateful to DMCU-UACJ for supporting his research stays at IPICyT (program PFCE and an academic mobility grant).

Appendix A. Supplementary data

Supplementary data to this article can be found online at https://doi.org/10.1016/j.jmmm.2021.168307.

References

[1] L. Wollmann, S. Chadov, J. Kubler, C. Felser, Magnetism in cubic manganese-rich Heusler compounds, Phys. Rev. B 90 (2014), 0.1103/PhysRevB.90.214420.
[2] S. Skaftouros, K. Ozdogan, E. Sasıoglu, I. Galanakis, Generalized Slater-Pauling rule for the inverse Heusler compounds, Phys. Rev. B 87 (2013), 0.1103/PhysRevB.87.024420.
[3] J. Ma, J. He, D. Mazumdar, K. Munira, S. Keshavarz, T. Lovorn, C. Wolverton, A. W. Ghosh, W.H. Butler, Computational investigation of inverse Heusler compounds for spintronics applications, Phys. Rev. B 98 (2018), 0.1103/PhysRevB.98.094410.
[4] F. Casper, C. Felser, R. Seshadri, C. P. Sebastian, and R. Pöttgen, Searching for hexagonal analogues of the half-metallic half-Heusler XYZ compounds, J. Phys. D: Appl. Phys. 41 (2008) 035002. 0.1088/0022-3727/41/3/035002.
[5] S.V. Faleev, Y. Ferrante, J. Jeong, M.G. Samant, B. Jones, S.S.P. Parkin, Origin of the tetragonal ground state of Heusler compounds, Phys. Rev. Applied 7 (2017) 034022, 1103/PhysRevApplied.7.034022.
[6] S. Keshavarz, N. Naghibolashrafi, M.E. Jamer, K. Vinson, D. Mazumdar, C. L. Dennis, W. Ratcliff II, J.A. Borchers, A. Gupta, P. LeClair, Fe2MnGe: a hexagonal Heusler analogue, J. Alloy. Compd. 771 (2019) 793–802, 0.1016/j.jallcom.2018.07.298.
[7] Q. Zhang, Z. Liu, J. Tan, X. Ma, Z. Cheng, Realization of tetragonal Heusler alloy Mn3-xCrxGa for spintronic applications, Intermetallics 108 (2019) 87–93, 0.1016/j.intermet.2019.02.013.
[8] C. Felser, A. Hirohata (Eds.), Heusler Alloys: Properties, Growth, Applications, Springer, Springer Series in Materials Science, Volume 222, Cham (2016) ISBN 978-3-319-21448-1 (DOI 10.1007/978-3-319-21449-8).
[9] I. Gavrikov, M. Seredina, M. Zheleznyy, I. Shchetinin, D. Karpenkov, A. Bogach, R. Chatterjee, V. Khovaylo, Magnetic and transport properties of Mn2FeAl, J. Magn. Magn. Mater. 478 (2019) 55-58. 0.1016/j.jmmm.2019.01.088.
[10] H.Z. Luo, H.W. Zhang, Z.Y. Zhu, L. Ma, S.F. Xu, G.H. Wu, X.X. Zhu, C.B. Jiang, H.B. Xu, Half-metallic properties for the Mn2FeZ (Z=Al, Ga, Si, Ge, Sb) Heusler alloys: a first-principles study, J. Appl. Phys. 103 (2008) 083908. 0.1063/1.2903057.
[11] F. Meng, X. Liu, Q. Li, H. Luo, Phase stability and magnetic properties of hexagonal and cubic Fe2MnGe, J. Magn. Magn. Mater. 482 (2019) 224-228. 0.1016/j.jmmm.2019.03.063.
[12] S. Ikeda, K. Miura, H. Yamamoto, K. Mizunuma, H.D. Gan, M. Endo, S. Kanai, J. Hayakawa, F. Matsukura, H. Ohno, A perpendicular-anisotropy CoFeB–MgO magnetic tunnel junction, Nature Materials 9 (2010) 721–724. 0.1038/nmat2804.
[13] J. Kim, H. Zhao, Y. Jiang, A. Klemm, J-P. Wang, C.H. Kim, Scaling analysis of in-plane and perpendicular anisotropy magnetic tunnel junctions using a physics-based model, 72nd Device Research Conference, Santa Barbara, CA (2014) pp. 155-156 (doi: 10.1109/DRC.2014.6872344).
[14] J. Rodríguez-Carvajal, Recent advances in magnetic structure determination by neutron powder diffraction, Physica B: Condensed Matter 192 (1993) 55–69.
[15] J.F. Qian, A K. Nayak, G. Kreiner, W. Schnelle, C. Felser, Exchange bias up to room temperature in antiferromagnetic hexagonal Mn3Ge, J. Phys. D: Appl. Phys. 47 (2014) 305001. 0.1088/0022-3727/47/30/305001.
[16] J. Crangle, The Magnetic Properties of Solids, Edward Arnold (publishers) Limited, London, 1977.
[17] A. Arrott, Criterion for ferromagnetism from observations of magnetic isotherms, Phys. Rev. 108 (1957) 1394. 0.1103/PhysRev.108.1394.